Title: **Hydration Effects Turn a Highly Stretched Polymer from an Entropic into an Energetic Spring**

Author(s): Liese, S., Gensler, M., Krysiak, S., Schwarzl, R., Achazi, A., Paulus, B., … Netz, R. R.

Document type: Postprint

Citation: This document is the Accepted Manuscript version of a Published Work that appeared in final form in ACS Nano, copyright © American Chemical Society after peer review and technical editing by the publisher. To access the final edited and published work see https://doi.org/10.1021/acsnano.6b07071.

Liese, S., Gensler, M., Krysiak, S., Schwarzl, R., Achazi, A., Paulus, B., … Netz, R. R. (2016). Hydration Effects Turn a Highly Stretched Polymer from an Entropic into an Energetic Spring. ACS Nano, 11(1), 702–712. https://doi.org/10.1021/acsnano.6b07071

Hydration Effects Turn a Highly Stretched Polymer from an Entropic into an Energetic Spring

Susanne Liese,[†] Manuel Gensler,[‡] Stefanie Krysiak,[¶] Richard Schwarzl,[†] Andreas Achazi,[§] Beate Paulus,[§] Thorsten Hugel,[‖] Jürgen P. Rabe,[‡] and Roland R. Netz[*,†]

Fachbereich für Physik, Freie Universität Berlin, 14195 Berlin, Germany, Department of Physics & IRIS Adlershof, Humboldt-Universität zu Berlin, 12489 Berlin, Germany, Physik Department and IMETUM, Technische Universität München, 85748 Garching, Germany, Institut für Chemie und Biochemie, Freie Universität Berlin, 14195 Berlin, Germany, and Institute of Physical Chemistry, University of Freiburg, 79104 Freiburg, Germany

E-mail: rnetz@physik.fu-berlin.de

Abstract

Polyethylene glycol (PEG) is a structurally simple and non-toxic water-soluble polymer that is widely used in medical and pharmaceutical applications as molecular linker and spacer. In such applications, PEG's elastic response against conformational deformations is key to its function. According to text-book knowledge, a polymer reacts to the stretching of its end-to-end separation by an decrease in entropy that is due to the reduction of available conformations, this is why polymers are commonly called entropic springs. By a combination of single-molecule force spectroscopy experiments with molecular dynamics simulations in explicit water, we show that entropic hydration effects almost exactly compensate the chain

[*]To whom correspondence should be addressed
[†]Fachbereich für Physik, Freie Universität Berlin, 14195 Berlin, Germany
[‡]Department of Physics & IRIS Adlershof, Humboldt-Universität zu Berlin, 12489 Berlin, Germany
[¶]Physik Department and IMETUM, Technische Universität München, 85748 Garching, Germany
[§]Institut für Chemie und Biochemie, Freie Universität Berlin, 14195 Berlin, Germany
[‖]Institute of Physical Chemistry, University of Freiburg, 79104 Freiburg, Germany

conformational entropy loss at high stretching. Our simulations reveal that this entropic compensation is due to the stretching-induced release of water molecules that in the relaxed state form double hydrogen bonds with PEG. As a consequence, the stretching response of PEG is predominantly of energetic, not of entropic, origin at high forces and caused by hydration effects, while PEG backbone deformations only play a minor role. These findings demonstrate the importance of hydration for the mechanics of macromolecules and constitute a case example that sheds light on the antagonistic interplay of conformational and hydration degrees of freedom.

Keywords: Polyethylene glycol, hydration, macromolecule elastic response, single-molecule force spectroscopy, molecular dynamics simulation

Polyethylene glycol (PEG) is used in a wide range of chemical, medical and technological applications.[1–5] It is the simplest water-soluble organic polymer and consists of the monomer unit -(CH_2-CH_2-O)- without any side chains. PEG is non-toxic and chemically inert and thus suitable in pharmaceutical applications as drug carrier,[6–8] spacer molecule[9,10] or as hydrogel formulation.[11,12] When end-grafted on surfaces it forms the basis of bioresistant and antifouling coatings.[13,14]

A crucial property of polymers is their elastic resistance against conformational deformations away from the unstretched equilibrium state. Polymers do not like to be compressed, this is why they can be used to build up osmotic pressure or to keep the proper distance between surfaces.[15–17] They also do not like to be extended, which is at the basis of rubber elasticity.[18] A number of simplified polymer models for the response to an external stretching force have been proposed: In the freely-jointed chain (FJC) model monomers are linked by stiff rods of fixed length without any angular constraints; since energetic effects are not taken into account the deformation penalty is purely entropic.[19,20] In the worm-like chain (WLC) model the chain contour is described as a continuous elastic line governed by bending energy;[21,22] also the stretching response of the WLC model is dominated by entropy while the energy in fact favors the extended state (see Supplement and our discussion below). This led to the general notion that polymers are entropic springs. Accordingly, a rubber band heats up when it is extended while it cools down when it is relaxed.[20,23] In all these theoretical models the molecular solvent is replaced by a homogeneous continuum

background within which a polymer moves, but it is not clear whether discrete solvent degrees of freedom modify or influence this simple picture in a significant way.

As has been shown earlier, water binds differently to PEG in the unstretched state compared to the stretched state.[24] While at low external stretching force single water molecules dominantly form two hydrogen bonds (HBs) with two neighboring oxygen atoms on the PEG backbone, in the high-force extended state solvation water predominantly forms single HBs.[24,25] These hydrogen-bonding properties of PEG have also been shown to give rise to rather complex phase behavior of PEG solutions as a function of temperature and pressure.[26] As we demonstrate in this paper by a tight combination of single-molecule atomic-force microscope (AFM) experiments and molecular dynamics (MD) simulations, doubly hydrogen-bonded water molecules lose significant orientational entropy compared to singly hydrogen-bonded hydration water. The gain in water orientational entropy due to the replacement of doubly by singly hydrogen-bonded hydration water almost exactly compensates the chain conformational entropy loss upon stretching. As a consequence, PEG turns from an entropic spring at low stretching to an energetic spring at high force. In fact, this energetic stretching response at high force is due to the release of hydration water, while the energetic contribution linked to PEG backbone deformations is negligible. This not only shows that water as a discrete solvent dictates the stretching thermodynamics of the simplest water-soluble polymer, it also opens ways to control and manipulate PEG conformation by thermodynamic means. PEG is a very simple polymer without side chains, but the mechanism of how solvation water entropically discriminates between folded and unfolded monomers presumably applies to all macromolecules where conformational change modifies the propensity of forming double hydrogen bonds with solvation water and is most likely not restricted to PEG. Our analysis starts with a quantitative comparison of MD simulations with experiments, which serves as a validation of our simulation model. For this comparison we performed single-molecule force spectroscopy experiments using two different experimental setups in the full force range from 10 pN to 700 pN. To eliminate a free fitting parameter in the comparison of experimental AFM data and MD simulations, we determine the vertical PEG grafting position on the AFM cantilever tip by comparison with ab initio high-force stretching curves. We also compare our MD simulations with previously published dynamic-light-scattering results for the radius of gyration of PEG coils in the absence of stretching force. For this comparison we determine the PEG Kuhn length from

MD low-force stretching curves. In both comparisons we obtain excellent quantitative agreement, which lends the necessary credibility to our further thermodynamics analysis of the PEG stretching simulations.

Results and Discussion

Force-extension relation of PEG:

In Figure 1a) the force-extension relation obtained from single molecule force-spectroscopy experiments (colored filled spheres) is shown. To demonstrate the robustness of our experimental results, we present results from two distinct experimental setups obtained with two different atomic-force microscopes (AFMs) and using two different anchoring chemistries (see Methods section). In the first setup a single PEG chain is covalently attached *via* one end to the AFM cantilever tip and adheres *via* a terminal dopamine-group to a TiO_2-surface (schematically depicted in Figure 1b). The second experimental setup employs a double-tether approach, where PEG chains are covalently bound to the AFM cantilever tip and to a gold surface *via* their ends and tightly adhere to each other *via* trivalent pyridine nanorods[27] (schematically depicted in Figure 1c); all measurements are performed in deionized water. In both experiments the tip-surface separation z is increased at fixed velocities and z as well as the force f exerted on the AFM cantilever are recorded.

Note that in order to allow for comparison with simulation data, in Figure 1a) we plot the force f *versus* the PEG end-to-end distance z_{ete} rescaled by the PEG contour length L. The experimental PEG segment number N is determined by the average molecular weight provided by the manufacturer, giving N=226 for the PEG chains used in the single-tether setup and N=427 for the sum of two chains in the double-tether setup (note that $N+1$ corresponds to the number of PEG monomers). This allows to calculate the experimental total contour length according to

$$L = a_0 N \tag{1}$$

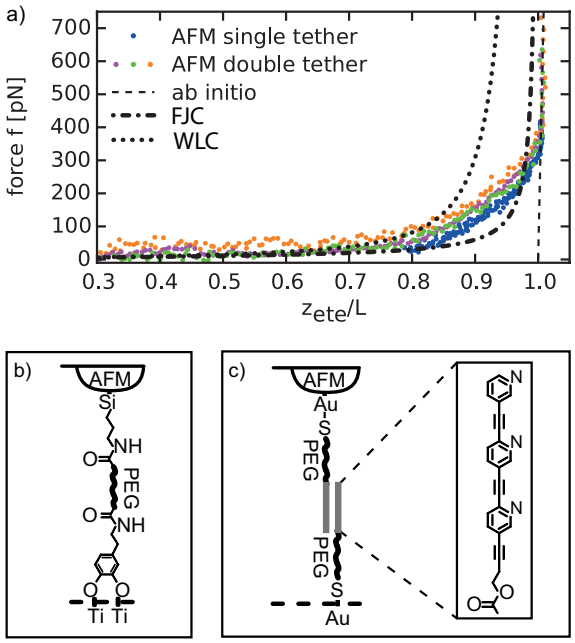

Figure 1: a) PEG stretching force data from AFM experiments (colored symbols). The AFM data come from two different setups that are schematically explained in subfigures b) and c). The PEG end-to-end distance z_{ete} is rescaled by the contour length L which follows *via* Eq. (1) from the segment number N and the equilibrium monomer length a_0. The dotted and dashed-dotted lines denote the worm-like chain (WLC) and the freely-jointed chain (FJC) predictions using the independently determined values for the contour length L and the Kuhn length b, both models obviously do not describe the PEG stretching behavior. b) Schematics of the experimental PEG single-tether setup. c) Schematics of the double-tether setup.

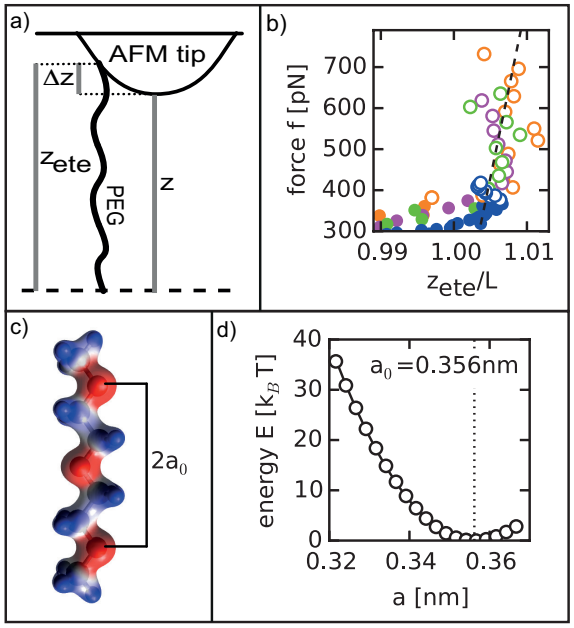

Figure 2: a) Schematics of the anchoring geometry on the AFM cantilever tip. The PEG anchoring position is displaced by a vertical shift Δz. b) The AFM data at strong stretching is compared with the ab initio quantum-chemical stretching force prediction (broken straight line). Only the AFM data for $f > 375$pN (denoted by open spheres) is fitted to the quantum-chemical stretching force and used to determine the vertical anchoring position Δz (schematically explained in a)) that relates the experimentally measured tip-surface separation z to the end-to-end separation $z_{\rm ete}$ *via* Eq. (2). c) Electrostatic potential distribution on an iso-electronic density surface of 2-methoxyethyl ether (CH_3-[O-CH_2-CH_2]$_2$-O-CH_3), which corresponds to the PEG unit-cell, in the equilibrium state with a monomer length of a_0=0.356nm from ab initio calculations. Negative potentials are shown in red, positive potentials in blue. d) Ground-state energy of 2-methoxyethyl ether per segment in vacuum from ab initio calculations as a function of the monomer length a. The minimum determines the equilibrium monomer length a_0=0.356nm (denoted by the vertical dotted line), the solid curve is a parabolic fit that determines the zero-temperature PEG stretching response, shown in subfigure b) as well as in Figure 1a) and Figure 3b) as straight broken lines.

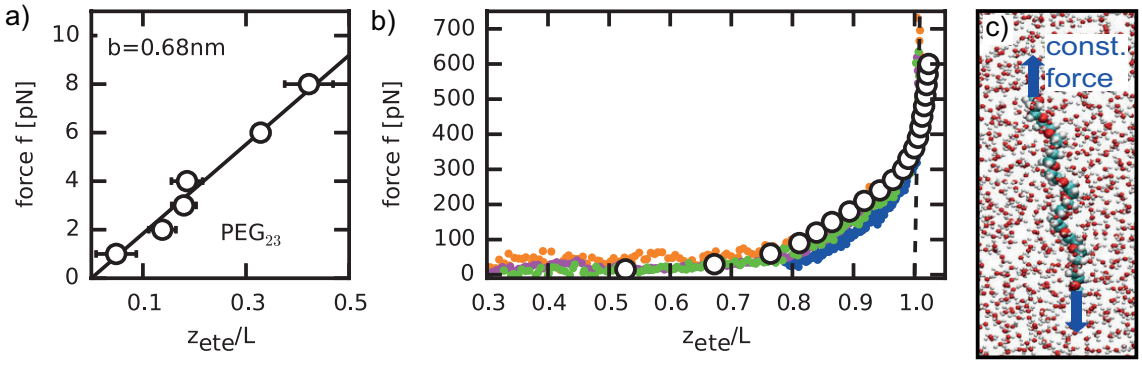

Figure 3: MD simulations of the PEG force-extension-relation: a) MD stretching force data for a PEG chain with $N = 23$ segments in the low force regime, the straight-line fit according to Eq. (3) yields a Kuhn length of $b = 0.68 \pm 0.02$nm. b) Comparison of PEG stretching force data from AFM experiments (colored symbols) and MD simulations (open symbols, N=11) over the entire force range. The same experimental data is shown in Figure 1a). The PEG end-to-end distance $z_{\rm ete}$ is rescaled by the contour length L which follows *via* Eq. (1) from the segment number N and the equilibrium monomer length a_0. c) Snapshot of the MD simulation for a PEG chain with $N = 11$ segments at a vertical stretching force of $f = 120$pN.

using the equilibrium PEG monomer length a_0 which we determine from ab initio quantum chemistry (AIQC) calculations (as will be explained below). However, the quantitative comparison of experimental and simulation data is subject to a subtle complication: The anchoring position of the PEG terminus on the cantilever tip is unknown and involves a vertical shift Δz, as schematically depicted in Figure 2a). Hence the measured tip-surface separation z does not equal the PEG end-to-end distance $z_{\rm ete}$ but rather is substantially reduced, and is described by the relation

$$z_{\rm ete} = z + \Delta z. \tag{2}$$

We determine the shift Δz by fitting the experimental force-extension data for stretching forces larger than 375pN (denoted by open spheres in Figure 2b) to the theoretical force-extension prediction from AIQC calculations (broken straight line). For this we determine the ground-state energy of 2-methoxyethyl ether, CH_3-[O-CH_2-CH_2]$_2$-O-CH_3, *i.e.* the PEG unit cell, as a function of the distance between the outer oxygen atoms, which corresponds to twice the PEG monomer length a, see inset in Figure 2c). Figure 2d) shows the total stretching energy per monomer $E(a)$, relative to the energy minimum, as a function of the monomer length a. The energy minimum determines the equilibrium monomer length a_0=0.356nm, which is used to calculate the PEG con-

tour length according to Eq. (1). We obtain $L = 80.5$nm in the single-tether and $L = 152.5$nm in the double-tether setup. The slope of the energy curve in Figure 2d), which is well fitted by a parabola (denoted by a solid line), corresponds to the stretching force f and is in Figure 2b) as well as in Figure 1a) and Figure 3b) denoted by a broken straight line. Note that the ab initio stretching curve is obtained in vacuum at zero temperature and thus solely results from bond stretching and bond angle deformations. The experimental data in Figure 2b) in fact converge nicely to the ab initio curve at elevated forces, showing that chain conformational fluctuations and solvent effects are negligible in the high-force limit.[28] The only fit parameter in the comparison in Figure 2b) is the vertical shift Δz, we find values for Δz between 20nm and 45nm (see Supplement for details of the fitting procedure). Compared to the PEG contour lengths used in our experiments, the vertical shifts are considerable, consequently it is important to correctly account for them in our analysis.

After determining the vertical shifts Δz and rescaling the experimental data by the contour length L, the experimental data for all measurements in Figure 1a) overlap over the whole force range, demonstrating that the force-extension-relation is a generic feature of PEG, independent of the anchoring chemistry, the contour length or the measurement setup. Our MD simulation results for a PEG chain consisting of $N = 11$ segments in explicit water, shown as black circles in Figure 3b), quantitatively agree with the experimental data over the entire force range. In the simulations, a constant force f in z-direction is applied to the chain ends and the averaged end-to-end-distance z_{ete}, defined as the distance between the outermost oxygen atoms projected along the force, is measured (see Figure 3c) for a simulation snapshot). We use the charmm35r force-field[29] that contains a modified O-C-C-O dihedral potential to improve the gauche-trans conformation ratio. In the current context it is interesting to note that the original charmm35 force field[30] was optimized based on thermodynamic quantities such as volume fraction and heat capacity of short ethers such as 1,2-dimethoxyethane. Our results demonstrate that charmm35r quantitatively describes the elastic properties of PEG chains over the entire force range. From the ab initio data in Figure 2d) an elastic stretching modulus of $\gamma = a_0 d^2 E(a)/da^2 = 89$nN is obtained, which is significantly higher than the stretching modulus obtained from MD simulations in vacuum and at zero temperature, $\gamma_{\mathrm{MD}} = 54$nN (see Supplement for details), which explains the smaller slope of the MD data in Figure 3b) compared to the ab initio data at forces larger than about 400 pN. We did not attempt to modify the MD force field to make up for this large-force behavior, mostly because

the effects we are after already show up at intermediate forces around 100pN.

Besides the contour length L, the other important polymer length scale is the Kuhn length. For an ideal polymer, the stretching response for small enough external force is linear and given by

$$z_{\mathrm{ete}}/L = bf/(3k_{\mathrm{B}}T), \tag{3}$$

which can be viewed as a definition of the Kuhn length b once the contour length L is known.[20,31] In Figure 3a) the MD-simulation force-extension relation for a PEG chain with $N = 23$ segments for forces smaller than 10pN is shown. A straight line fit according to Eq. (3) yields a Kuhn length of $b = 0.68 \pm 0.02$nm. The Kuhn length b turns out to be roughly twice the monomer length a_0, which is in reasonable agreement with theoretical predictions for a homogeneous freely rotating chain model.[32,33] This is different from the case of peptides, for which the inhomogeneous chemical backbone structure has been shown to lead to a considerably increased Kuhn length because of restricted dihedral rotations.[34]

The force-distance relations for the WLC and FJC models are in Figure 1a) included as dotted and dashed-dotted lines, respectively (see Supplement for the explicit expressions). Note that in this comparison the Kuhn length $b = 0.68$nm is taken from the low-force fit of the MD simulation data in in Figure 3a), which *via* the relation $\ell_p = b/2$ also determines the persistence length ℓ_p of the WLC model.[32] So there is actually no free fitting parameter in this comparison, since the PEG contour length L is independently determined from the experimental large-force data in Figure 2b) by comparison with the quantum-chemical stretching response. We see that both models fail to describe the PEG stretching behavior even qualitatively. Interestingly, the FJC as well as the WLC model fits the experimental data very well when Kuhn length and contour length are used as free fitting parameters (see Supplement). On the one hand, this explains why the WLC model is commonly used to fit experimental PEG stretching data.[35–37] On the other hand, this demonstrates that the short coming of standard polymer stretching models is only revealed when the fundamental polymer length scales b and L are determined independently, as is the case in Figure 1a). These results for PEG are different from the classical example of DNA stretching, where the FJC model fails but the WLC chain model correctly describes the DNA stretching data over the entire force range.[21] The reason is that the DNA Kuhn length reaches 100 nm and thus is the by far largest

length scale in the problem. For PEG, the Kuhn length b is less than a nanometer and thus of the same order as the segment length a_0, which is the scale at which solvation effects come in, as we will explicitly demonstrate below.

Equilibrium size of PEG coils:

To further validate our MD simulations, we present the average end-to-end distance $R_{\rm ete}$ (measured between the outermost oxygen atoms) in the absence of an external stretching force as a function of segment number N ranging from $N = 1$ to $N = 23$ in Figure 4a) . For an ideal chain, *i.e.* in the absence of interactions between polymer monomers, the average end-to-end distance $R_{\rm ete}$ scales as[20]

$$R_{\rm ete}^{\rm ideal} = \sqrt{b a_0 N}. \tag{4}$$

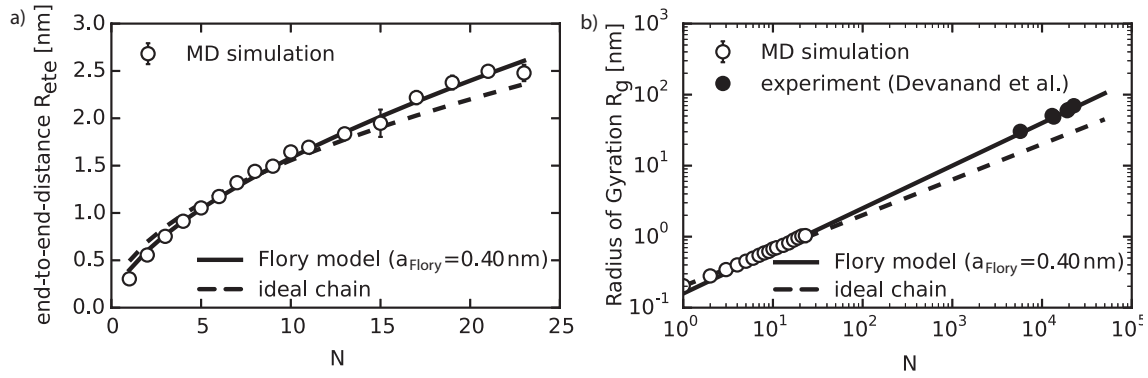

Figure 4: Equilibrium size of PEG coils: a) MD simulation results for the end-to-end distance $R_{\rm ete}$ of PEG as a function of the segment number N. The ideal-chain prediction Eq. (4) with the monomer length $a_0 = 0.356$nm taken from ab initio calculations in Figure 2d) and the Kuhn length $b = 0.68$nm from the fit in Figure 3a) is shown as a broken line. The solid line shows a fit according to the Flory model Eq. (5) yielding an effective monomer length $a_{\rm Flory} = 0.40 \pm 0.004$nm. b) Comparison of the radius of gyration $R_{\rm g}$ from MD simulations (open spheres) and light scattering experiments[38] (filled spheres) in a double-logarithmic plot. The ideal and Flory predictions (broken and solid lines, respectively) follow from the relations $R_{\rm g}^{\rm ideal} = R_{\rm ete}^{\rm ideal}/\sqrt{6}$ and $R_{\rm g}^{\rm Flory} \simeq 0.398 R_{\rm ete}^{\rm Flory}$ using the results for $R_{\rm ete}$ from a).

Using the value b=0.68nm for the Kuhn length previously determined from the low-force MD stretching data in Figure 3a) and the value $a_0 = 0.356$nm from the ab initio calculations, we see in

Figure 4a) that the simulation data follow the ideal chain behavior (broken line) with only minor deviations for large N, without invoking an additional fitting parameter. In fact, self-avoidance effects and repulsive interactions between monomers modify the scaling of R_{ete} according to the Flory model,[19,39]

$$R_{\rm ete}^{\rm Flory} = a_{\rm Flory} N^{3/5}, \tag{5}$$

where the effective monomer length $a_{\rm Flory}$ depends on the monomer-monomer interaction parameters (*i.e.* the second virial coefficient) and the Kuhn and monomer lengths in a complex manner.[20] From a fit of Eq. (5) to the MD data in Figure 4a), indicated by a solid line, we obtain a value of $a_{\rm Flory} = 0.40 \pm 0.004$nm, we also see that the Flory law Eq. (5) describes the MD data slightly better than the ideal scaling law Eq. (4). In Figure 4b) we compare the radius of gyration $R_{\rm g}$ from MD simulations (open circles), obtained from the definition $R_{\rm g}^2 = \sum_{i,j}(r_i - r_j)^2/(2N^2)$ *via* a double sum over the monomer positions r_i, with experimental light scattering data.[38] We also include the scaling laws following from the fits in Figure 4a) *via* the relations $R_{\rm g}^{\rm ideal} = R_{\rm ete}^{\rm ideal}/\sqrt{6} \simeq 0.408 R_{\rm ete}^{\rm ideal}$ for an ideal chain and $R_{\rm g}^{\rm Flory} \simeq 0.398 R_{\rm ete}^{\rm Flory}$ for a self-avoiding chain.[40] Note that the power laws indicated in Figure 4b) by straight lines do not result from a fit but rather follow from the parameters of the curves shown already in Figure 4a). From the comparison in Figure 4b) it transpires that the MD data, when extrapolated according to a self-avoiding chain, is in perfect agreement with experimental scattering data, validating our simulation model also in terms of the equilibrium (*i.e.* unstretched) behavior of long PEG chains.

Thermodynamics of stretched PEG:

Having validated our PEG simulation model and our simulation techniques by quantitative comparison with experimental data for strongly stretched as well as for unstretched (equilibrium) chains, we are now in a position to unravel the thermodynamic signature of PEG stretching, the key question of this paper that is difficult to address directly in experiments.[41] By integration of the simulated PEG force-extension relation we obtain the free energy change with respect to the force-free reference state for $f = 0$ as $F(z_{\rm ete}) = \int_0^{z_{\rm ete}} f(z'_{\rm ete}) dz'_{\rm ete}$. We also calculate from the simulation trajectory the total energy change U and from that the change of the entropy contribution to the free energy $TS = U - F$. All three quantities are in Figure 5a) shown per PEG segment as a function of

the applied force f (data points). Strikingly, the free energy F is given almost entirely by the energy U and the entropy contribution $-TS$ is positive but very small. Interestingly, $-TS$ (green data points) exhibits an initial increase for small forces, passes through a minimum around $f \approx 200$pN and increases weakly for larger force but is strictly smaller than $1k_BT$.

In Figure 5b) we compare the relative energy U/F (red squares) with the relative entropy contribution $-TS/F$ (green triangles). This presentation shows that the PEG stretching entropy is dominant for forces smaller than 100pN but becomes negligible for larger forces. The comparison with standard polymer models brings further insight: In the freely-jointed chain (FJC) model the stretching free energy is entirely due to entropy, and thus $U/F = 0$ while $-TS/F = 1$, independent of force, as indicated by red and green broken horizontal lines, in stark contrast to the MD data. The worm-like chain (WLC) model describes a polymer as a continuous elastic line and is the preferred model for describing the stretching response of synthetic as well as biological polymers.[22,42,43] Since the WLC elastic energy decreases with rising force and reaches zero in the infinite force limit, the relative entropy contribution $-TS/F$ is even higher than in the FJC model. In fact, a simple calculation (fully presented in Supplement) shows that in the WLC model one has U/F=-1 and $-TS/F$=2 (red and green dotted horizontal lines), disagreeing even more vividly (including the force-free limit) with the MD data. As we will show below, the non-standard thermodynamic signature of PEG stretching is caused by the coupling of PEG conformational and solvent degrees of freedom, not by energetic properties associated with backbone elasticity.

In Figure 5c) the fraction of PEG monomers in trans-conformation, ϕ_{trans}, as determined by the O-C-C-O dihedral angle ψ, is shown. At zero external force monomers are predominantly in a gauche-conformation and ϕ_{trans}=4%, while ϕ_{trans} increases continuously with rising force and reaches ϕ_{trans}=98% at a force of f=600pN. The gauche-trans transition of PEG monomers thus reflects a conformational transformation of PEG as the stretching force increases, in agreement with previous results.[24,25,44–46]

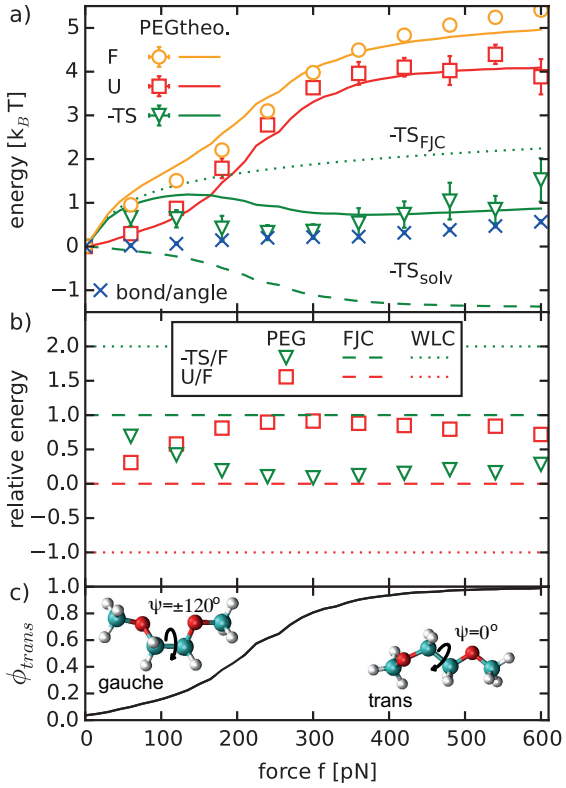

Figure 5: Thermodynamics of a stretched PEG chain: a) Decomposition of the MD stretching free energy F per PEG segment into energy U and entropy contributions $-TS$ (data points). The solid lines show model estimates that include solvation effects according to Eq. (6), Eq. (9), Eq. (10). The dotted line shows the entropy of the FJC model, $-TS_{\mathrm{FJC}}$, Eq. (8), while the broken line shows the pure solvation entropy contribution $-TS_{\mathrm{solv}}$, Eq. (7). The blue crosses show the energetic PEG backbone contribution, due to bond length and bond angle deformations, which is rather negligible over the entire force range. b) Relative stretching energy U/F and stretching entropy $-TS/F$ from simulations (data points) compared with FJC (horizontal broken lines) and WLC predictions (horizontal dotted lines). c) The fraction of PEG segments in the trans conformation ϕ_{trans} increases with increasing force.

Thermodynamics of the gauche-to-trans transition of a single PEG monomer:

To connect the PEG-monomer gauche-trans transition with the thermodynamics of the stretching response of an entire PEG chain, we need an in-depth understanding of the thermodynamic response of the water degrees of freedom upon external force application. This is not possible using the MD simulations of entire PEG chains. The shortest PEG section that contains an O-C-C-O dihedral is 1,2-dimethoxyethane (DME: CH_3-O-CH_2-CH_2-O-CH_3). Figure 6a) shows the DME free energy landscape $F_{\mathrm{DME}}(d_{\mathrm{OO}})$ as a function of the oxygen-oxygen distance d_{OO} from umbrella MD simulations[47] of a single DME in water. Note that $F_{\mathrm{DME}}(d_{\mathrm{OO}})$ by construction does not contain the conformational PEG backbone entropy associated with the gauche-to-trans transition of individual PEG segments. It therefore allows to concentrate the discussion on pure solvation effects. The two pronounced free energy minima at d_{OO} =0.3nm and d_{OO} =0.367nm correspond to the gauche- and trans-conformations, respectively. The gauche conformation is in the absence of external force favored over the trans state by a free energy difference of ΔF_{DME}=2.8k$_B$T, as can be read off from the two broken horizontal lines through the free energy minima.

This resonate well with our finding in Figure 5c) that only ϕ_{trans}=4% of PEG monomers are in the trans state at zero force. In fact, the simulation result ϕ_{trans}=4% is not too far off from the simple Boltzmann estimate for the trans-state probability $e^{-2.8}/(1+e^{-2.8}) \simeq 0.06$ using the DME free energy difference ΔF_{DME}=2.8k$_B$T. To decompose the free energy change ΔF_{DME} into solvent entropy and energy, we perform MD simulations in which the dihedral angle ψ is harmonically constraint to ψ=120$\pm$5^o, corresponding to the gauche state, and ψ=0$\pm$5^o, the trans state. The two resulting approximately Gaussian probability distributions are shown in Figure 6a) by dashed-dotted curves, confirming that our ψ-constrained simulations successfully single out the gauche- and trans-conformation ensembles. The thermodynamic decomposition of ΔF_{DME} in Figure 6b) shows that while the energy difference ΔU_{DME} is positive, the entropy contribution $-T\Delta S_{\mathrm{DME}}$ indeed is negative, *i.e.*, the entropy, which is entirely due to solvent degrees of freedom, increases significantly when going from the gauche to the trans state. The further decomposition of the energy according to $\Delta U_{\mathrm{DME}} = U_{\mathrm{PP}} + U_{\mathrm{PW}} + U_{\mathrm{WW}}$ shows that both PEG-PEG and water-water-interactions prefer the trans conformation, since $U_{PP} < 0$ and $U_{WW} < 0$, however the total energy is dominated by the much larger PEG-water contribution $U_{PW} > 0$ which prefers the gauche state.

We conclude that it is the PEG-water interaction which favors the more compact gauche state on a purely energetic basis. This is quite counter-intuitive since PEG is polar and one would expect that the compact gauche state should be favored by PEG-PEG interactions while the extended trans state should be favored by PEG-water interactions.

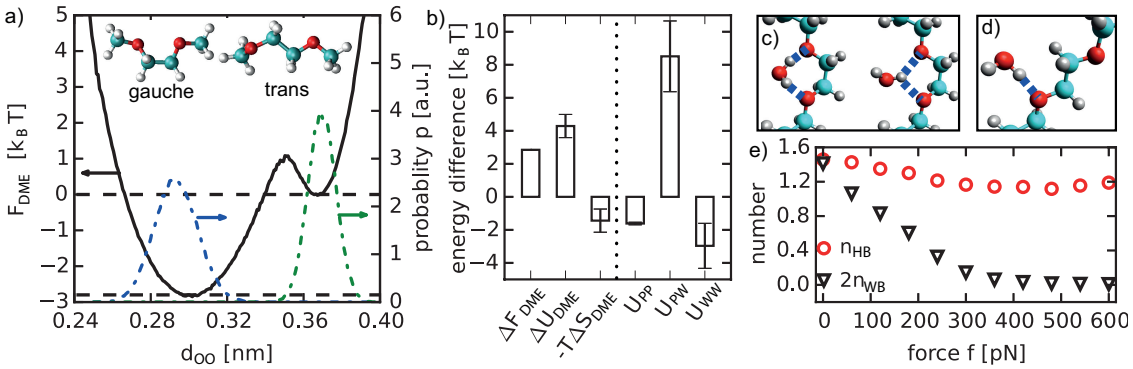

Figure 6: Thermodynamics of a single PEG monomer: a) Free energy of 1,2-dimethoxyethane (DME) in water in dependence of the distance between the oxygen atoms d_{OO}, determined from MD umbrella simulations (black solid curve). The left minimum corresponds to the gauche conformation, while the right minimum corresponds to the trans conformation. The probability distributions $p(d_{\mathrm{OO}})$ employed in our constrained simulations at dihedral angles ψ=0$\pm$5^o and ψ=120$\pm$5^o are shown in blue and green. b) Energy decomposition for the transition of a single DME from gauche to trans. The free energy difference ΔF_{DME} is obtained from the free energy profile in a). To determine the internal energy change ΔU_{DME} constrained simulations at fixed dihedral angles ψ=0$\pm$5^o and ψ=120$\pm$5^o are performed. The internal energy change is furthermore decomposed into PEG-PEG (PP), PEG-water (PW) and water-water (WW) interactions according to $\Delta U_{\mathrm{DME}} = U_{\mathrm{PP}} + U_{\mathrm{PW}} + U_{\mathrm{WW}}$. c) Schematic picture of a water bridge with two (left) and one (right) hydrogen involved. d) Schematic picture of a water configuration forming a single hydrogen bond with PEG. e) Total number of hydrogen bonds, n_{HB}, and total number of water bridges (multiplied by two), $2n_{WB}$, per segment for a PEG chain with $N = 11$ segments in dependence of the applied force.

These thermodynamic results can be microscopically understood from the number of PEG-water hydrogen bonds n_{HB} and water bridges n_{WB}. Here we denote a water bridge as a water molecule that forms two hydrogen bonds with PEG, this can either involve both hydrogens of a single water molecule, as indicated in Figure 6c) on the left side, or only a single water hydrogen, see Figure 6c) to the right. While the number of water bridges per PEG monomer n_{WB} in Figure 6e) (black triangles) decreases strongly with increasing force and vanishes at forces larger than $f \simeq 400$pN, the total number of PEG-water HBs per monomer n_{HB} (red spheres) decreases only slightly with rising

force and saturates at a finite value at large force. In fact, for zero force the total number of hydrogen bonds n_{HB} equals twice the number of water bridges (note that we plot $2n_{\mathrm{WB}}$ in Figure 6e)), meaning that at zero force all PEG-water hydrogen bonds come from water bridges, in agreement with previous MD simulations[24,48] as well as ab initio calculations.[25] For large force we find $n_{WB} \approx 0$, meaning that all HBs come from singly coordinated water molecules. The replacement of doubly coordinated water molecules by singly hydrogen-bonded water molecules we associate with the entropy gain when going from gauche to trans: from the value $T\Delta S_{\mathrm{DME}} \simeq 1.4 k_{\mathrm{B}}T$ in Figure 6b) and the number of water bridges per PEG segment at zero force $n_{\mathrm{WB}} \simeq 0.71$ in Figure 6e), we conclude that an entropy contribution of roughly $TS_{\mathrm{WB}} = T\Delta S_{\mathrm{DME}}/0.71 \simeq 2k_{\mathrm{B}}T$ is gained per released water bridge when going from gauche to trans. This is a very plausible value when we assume that a water bridge is, due to double hydrogen bonding, restricted in its orientational freedom around one rotational axis: Using the statistical mechanics definition of the entropy change of a continuous angular degree of freedom,[49] we reproduce the estimated value of $TS_{\mathrm{WB}} \simeq 2k_{\mathrm{B}}T$ by assuming a rotational angle restriction down to roughly 50^o degrees compared to free rotation through 360^o degrees, yielding an angular entropy cost of $TS_{\mathrm{WB}} = k_{\mathrm{B}}T\ln(360^o/50^o) \approx 2k_{\mathrm{B}}T$. This simple example shows that even moderate angular restrictions of molecular degrees of freedom can lead to sizable entropy contributions.

Simple thermodynamic model for the stretching of solvated PEG chains:

We now establish the connection between the thermodynamic results for the gauche-trans transition of DME and our MD stretching results for entire PEG chains in water. In Figure 5a) we plot the force-dependent PEG solvation energy per segment

$$U_{\mathrm{solv}} = \Delta U_{\mathrm{DME}} \Delta\phi_{\mathrm{trans}}(f), \tag{6}$$

which we express as the product of the DME gauche-trans energy change $\Delta U_{\mathrm{DME}} = 4.2 k_{\mathrm{B}}T$ from Figure 6b) and the force-induced fraction of trans conformations $\Delta\phi_{\mathrm{trans}}(f) = \phi_{\mathrm{trans}}(f) - \phi_{\mathrm{trans}}(f = 0)$ from Figure 5c), as a solid red line. The agreement with the PEG stretching energy simulation data (red squares) is excellent, which demonstrates that the PEG stretching energy is a solvation effect solely due to water-PEG binding. The blue crosses in Figure 5a) denote the energetic PEG

backbone contribution, which is due to bond length and bond angle deformations. The PEG backbone energy is rather small over the entire force range and starts to make a sizable contribution only for forces larger than $f > 500$pN, which confirms that the PEG stretching energy in water is due to solvation effects, not due to stretching of the PEG backbone.

We furthermore plot

$$TS_{\rm solv} = T\Delta S_{\rm DME}\Delta\phi_{\rm trans}(f) \tag{7}$$

as a broken green line in Figure 5a), which is negative and describes the solvation entropy gain as PEG is stretched.

The configurational stretching entropy penalty of a FJC model

$$\begin{aligned} TS_{\rm FJC} = & \frac{k_{\rm B}Ta_0}{b}\left[\ln\left(\frac{4\pi bk_{\rm B}T}{f}\sinh\left(\frac{fb}{k_{\rm B}T}\right)\right)\right. \\ & \left. -\frac{fb}{k_{\rm B}T}\left(\coth\left(\frac{fb}{k_{\rm B}T}\right)-\frac{k_{\rm B}T}{fb}\right)\right] \end{aligned} \tag{8}$$

is the standard Langevin result[50] for a rigid rotor of Kuhn length b under external stretching force (the derivation is fully presented in the Supplement). We take for the Kuhn length $b = 0.68$nm, and the prefactor a_0/b reflects that in Figure 5a) we show all energies per PEG segment of length a_0 while the effective FJC model is properly formulated in terms of the Kuhn length b. The FJC entropy contribution $-TS_{\rm FJC}$, shown as a dotted green line in Figure 5a), is positive and for large forces reaches a value of $2k_{\rm B}T$. Not only is the FJC contribution much smaller than the actual MD stretching free energy (yellow data points), it also is a very poor description of the simulated entropy (green data points). The sum of the solvation and FJC entropy contributions,

$$TS_{\rm FJC+solv} = TS_{\rm solv} + TS_{\rm FJC}, \tag{9}$$

shown by a solid green line in Figure 5a), describes the simulation entropy data fairly well for small as well as for large forces. This graphically demonstrates that the almost complete absence of stretching entropy effects in the simulation data at large force is due to a near cancellation of conformational and solvation entropy.

The theoretical estimate for the total free energy

$$F_{\mathrm{FJC+solv}} = U_{\mathrm{solv}} - TS_{\mathrm{solv}} - TS_{\mathrm{FJC}}, \tag{10}$$

which combines the solvation solvation free energy and the FJC stretching entropy, indicated by a yellow line in Figure 5a), describes the simulated PEG stretching free energy very well. In conclusion, the FJC model is not invalid, but the configurational entropy penalty predicted by the FJC model is almost exactly compensated by the solvation entropy gain at large forces. The main contribution to the stretching free energy is due to the solvation energy, while the energy associated with the stretching of the PEG backbone is in fact rather negligible.

Conclusion

We present a quantitative comparison of PEG chain MD simulations in explicit water with two different experiments. AFM force spectroscopy on the one hand probes PEG conformations under strong external force, light scattering measurements on the other hand probe the equilibrium PEG conformational behavior in the absence of external stretching force. The quantitative agreement of MD simulation results with both experiments validates the charmm35r force field used by us as well as the general simulation setup employed. Our thermodynamic analysis of the simulation results demonstrates that PEG at moderate to strong stretching forces acts as an energetic elastic chain with only negligible entropy contributions. This stands in stark contrast to standard polymer stretching models, which all predict the conformational entropy to be the dominant ingredient to the polymer stretching response. We explain the PEG stretching thermodynamics quantitatively by an in-depth analysis of the solvation behavior of a PEG dimer, where we see that water doubly coordinates to PEG oxygens and forms water bridges in the unstretched gauche state. As PEG is stretched, these doubly coordinated water molecules are replaced by singly coordinated water molecules, which releases an entropy contribution TS of roughly $2k_{\mathrm{B}}T$ per water bridge. This entropy gain of released water bridges almost perfectly compensates the conformational entropy penalty of PEG stretching, explaining why PEG is not an entropic spring at high forces. On the other hand, the energetic cost of destroying the water bridges is about $4k_{\mathrm{B}}T$ per PEG monomer,

which quantitatively explains the energetic stretching behavior of PEG in water. Surprisingly, the energetic contribution from the PEG backbone elasticity is rather negligible, so we find that solvation effects completely dominate the stretching response of PEG to large forces.

Our findings have numerous consequences. Water bridges, which are the prevalent hydration mode for unstretched PEG, have a high entropy cost and thus become unfavorable at high temperatures. This explains why PEG solvation becomes unfavorable at high temperatures and thus the tendency of PEG monomers to aggregate increases.[26,51,52] Intra-chain aggregation induces the collapse of single PEG chains, while inter-chain aggregation leads to the phase separation of PEG gels and solutions. The thermodynamic signature of the water-bridge solvation mechanism unveiled here is somewhat similar to the hydrophobic effect: the solvation free energy of small hydrophobic solutes is maximal at a characteristic temperature and thus (for low enough temperature) increases with rising temperature due to the entropy loss of the water hydrogen bond network around the solute.[53–56] But the microscopic mechanisms behind these similar thermodynamic solvation features are very different: While for hydrophobic solutes the solvation entropy cost comes from water forming water-water hydrogen bonds around the solute, for PEG in the relaxed state the entropy cost comes from the proliferation of entropically costly doubly coordinated water bridges between solvation water and PEG oxygens. Thus, the mere presence of solvation entropy contributions does not allow to distinguish hydrophobic solvation effects from the double-hydrogen bonding hydration mechanism which is predicted when the solute bears hydrogen bond acceptors at the proper distance.

Strongly stretched PEG structures are encountered when PEG is used as linker or tether.[57,58] The absence of stretching entropy implies that the stretching free energy is rather temperature independent, which is important for the design of macromolecular constructs that have to function over a wide temperature range. In the Supplement we show simulated PEG stretching curves at different temperatures and explicitly demonstrate that the stretching force at moderate to large PEG extension is rather constant over a temperature range from 250 to 400 K. In future work these simulation results shall be compared with AFM experiments at different temperatures.

The fundamental lesson learned from our studies is twofold: First, since polymer force-stretching curves are rather smooth and without pronounced characteristic features, short comings of polymer stretching models (such as the WLC or the FJC model) can only be detected if the two model

parameters (contour length and Kuhn or persistence length) are determined independently. As shown in the Supplement, the WLC model almost perfectly describes the PEG force-stretching curve if Kuhn length and contour length are free fit parameters. In our approach, the Kuhn length is extracted from the low-force stretching response and matches the experimental equilibrium coil size. The contour length is a more subtle parameter, since in AFM experiments with short polymers the polymer anchoring position on the AFM cantilever introduces an unknown shift of the polymer end-to-end distance even if the polymer weight is precisely known. We here show that the anchoring position can be fitted by comparison with the quantum chemistry stretching force at high forces. Once Kuhn length and contour length are known and the anchoring position on the cantilever is determined, PEG is shown to be neither described by the FJC nor the WLC model.

Secondly, deviations from standard polymer models, which are particularly large for polymers that show conformational transitions upon stretching such as PEG (as discussed here) or carbohydrates,[59] need not necessarily be linked to energetic backbone stretching events. Rather, for PEG, solvation effects are pronounced and completely dominate over the backbone stretching energy as well as the polymer configurational entropy.

We finally speculate that the water-bridge mechanism is also relevant for the solvation of other uncharged polar polymers such as glycopolymers and polypeptides, and might be an important ingredient to explain the often peculiar temperature-dependence of macromolecular solvation in water.[60,61]

Methods

Experiments: Two sets of polymer-stretching measurements are performed to determine the force-extension relation of PEG. For the first set of measurements TiO_2 slides are prepared by sputtering titanium on silica wafers as described previously.[62] The PEG chains are grafted to the tip through covalent bonds in a similar manner as described previously.[63] Silicon nitride cantilevers (MLCT, Bruker SPM probes, Camarillo, USA) are first activated in an oxygen plasma chamber (20W, 0.3mbar) for 15 min. Cantilevers are rinsed with dry acetone (VWR, Germany) and then incubated for 10 min in a Vectabond (Axxora, Germany) solution (50 μl Vectabond in 2.5 ml dry acetone) for silanization. Afterwards they are rinsed in dry acetone and dry chloroform (VWR, Germany).

PEG-α-ω-Di-NHS (10 kDa, Rapp Polymere GmbH, Tübingen, Germany) is dissolved in dry chloroform (2.5mM) and the cantilevers are incubated for 60 min. The cantilevers are now rinsed in dry chloroform, ethanol and afterwards incubated for 1 h in dopamine solution (Sigma Aldrich, 1mg/ml dissolved in 50mM sodium-borate buffer, pH 8.1). The AFM force spectroscopy measurement with the functionalized tip is carried out with an MFP-3D (Oxford Instruments) equipped with a fluid cell at room temperature. The measurement is done in double distilled water on TiO_2. The tip is moved towards the surface at constant velocity, held at the surface for a dwell time of 1 s and retracted at a constant velocity of 1μm/s. The catechol group of the attached dopamine adheres to the TiO_2 surface so that the PEG chain is stretched during retraction of the tip. The inverse optical lever sensitivity (InvOLS) of the functionalized cantilever is determined from the indentation slope and the spring constant is calibrated by the thermal noise method according to.[64] For the second set of measurements Pyridine-PEG conjugates (as shown in Figure 1c)) are synthesized and surface films of the polymers are prepared as described before.[27] In short, a 1 mM solution of the polymer in water is applied to gold coated silicon nitride cantilevers (Olympus Biolever A, Olympus Cooperation, Tokyo, Japan) and template stripped surfaces (JPK Instruments, Berlin, Germany) for 12-24 h at room temperature. Afterwards surface and cantilever are rinsed thoroughly with water. Experiments are performed on a ForceRobot 200 (JPK Instruments, Berlin, Germany) at room temperature in Milli-Q water. Cantilever probes are calibrated using the thermal noise method.[65] Measurements are performed at various retract speeds ranging from 100 nm/s to 10μm/s on various spots of the surface. We detected no dependence on pulling speed (see Supplement), indicating pulling in the equilibrium regime.[46] Simultaneous pulling events of two or more PEG chains are excluded by only using sawtooth-signals that do not show any additional peaks in between half and the maximum linker length. Only the last peak in each force-distance curve is taken into consideration for further analysis. In our analysis we neglect the effect of tilted polymer stretching since the typical lateral chain dimension is much smaller than the stretched end-to-end distance.

Ab initio calculations: The conformation of 2-methoxyethyl ether with constrained terminal oxygen positions is optimized with the Gaussian package[66] using the DFT-functional m06-2x[67] with the basis set aug-cc-pVTZ.[68]

Molecular Dynamics simulations: All MD simulation are performed with the GROMACS sim-

ulation package.[69] If not indicated otherwise the following simulation parameters are used: The time step is set to 2 fs. The temperature is set to 300K. For temperature-/pressure coupling the v-rescale[70]/Parrinello-Rahman[71] algorithm with a relaxation time of 0.1ps/0.5 ps is chosen. The pressure is set isotropically to 1 bar with a water compressibility of $4.5 \cdot 10^{-5}$bar^{-1}. All simulations are performed with periodic boundary conditions in all three directions. The cut-off of non bonded interactions is set to 1.0nm. Long range electrostatic interactions are treated with the PME method. The length of all bonds between oxygen and hydrogen are fixed. To mimic the AFM-measurements an elongated chain (H-[CH_2-O-CH_2]$_{12}$-H) is placed in a 3.5nm x 3.5nm x 10nm box filled with 3970 tip3p water molecules. To equilibrate the system the minimization is followed by a 10ps NVT simulation with constant volume and without pressure coupling and a 2ns NPT-simulation with an isotropic pressure of 1bar. For the production run the first and the last oxygen atoms are defined as pulling groups. A constant force between 1pN and 600pN is applied in z direction. The pulling simulation is performed for 20ns up to 200ns. To check for possible hysteresis effects, we determined the relaxation time of the end-to-end distance and the relaxation time of the number of water bridges as a function of the applied force. For all systems the relaxation time is much shorter than the simulation time, so that non-equilibrium hysteresis effects can be safely excluded in our simulations (see Supplement for details). The first 500ps are discarded in the analysis. The end-to-end distance is calculated between the first and last oxygen atoms and averaged over time. For the low force regime a H-[CH_2-O-CH_2]$_{24}$-H chain is placed in a 4.5nm x 4.5nm x 10.5nm box. After equilibration a constant force between 1pN and 8pN is applied in z direction for 200ns. The first ns is discarded in the analysis. The free energy F is obtained by integrating over the force-extension-relation, while the internal energy U is determined from the interaction potential between all components of the system. Hydrogen bonds are determined based on a geometric definition, with a donor-acceptor distance of 0.3nm and a donor-hydrogen-acceptor angle of 120^o.[72] A water molecule that forms two hydrogen bonds with PEG is denoted as water bridge. To study the radius of gyration, a PEG chain H-[CH_2-O-CH_2]$_{N+1}$-H, with N=1 to N=23 is placed in a cubic box of length 2.3nm to 6.2nm. To equilibrate the system the energy minimization is followed by a 10ps NVT simulation with constant volume and without pressure coupling and a 2ns NPT-simulation with an isotropic pressure of 1bar. For the production run a 100ns NPT simulation is performed. For the umbrella sampling DME is placed in a 2.435x2.361x2.602nm^3 box with 470

water molecules. After energy minimization the box is equilibrated for 100ps in a NPT simulation. Afterwards a harmonic potential with a force constant of 20000kJ/(mol nm^2) is applied between the oxygen atoms. The minimum of the harmonic potential is varied between 0.25nm and 0.39nm in steps of 0.021nm. The simulations are analyzed with the WHAM algorithm.[47] The first 50ps of each simulation are discarded. To determine the internal energy two simulations are performed to constrain the O-C-C-O dihedral angle to 0^o and 120^o with a harmonic constrain potential with a force constant of 325kJ/(deg^2).

Acknowlegement

This contribution was generously supported by the Deutsche Forschungsgemeinschaft DFG *via* grant SFB 765 and SFB 1112. The High-Performance Computing facilities of the Freie Universität Berlin (ZEDAT) is acknowledged for supercomputing access.

Supporting Information Available

Further discussions of the experimentally measured and simulated force-extension curves as well as the derivation of the energy decomposition of the FJC and WLC model are given in the Supporting Information. This material is available free of charge *via* the Internet at http://pubs.acs.org/.

References

1. Langer, R.; Tirrell, D. Designing Materials for Biology and Medicine. *Nature* **2004**, *428*, 487–492.

2. Welsher, K.; Liu, Z.; Sherlock, S. P.; Robinson, J. T.; Chen, Z.; Daranciang, D.; Dai, H. A Route to Brightly Fluorescent Carbon Nanotubes for Near-Infrared Imaging in Mice. *Nature Nanotech.* **2009**, *4*, 773–780.

3. Brandenberger, C.; Muehlfeld, C.; Ali, Z.; Lenz, A.-G.; Schmid, O.; Parak, W. J.; Gehr, P.; Rothen-Rutishauser, B. Quantitative Evaluation of Cellular Uptake and Trafficking of Plain and Polyethylene Glycol-Coated Gold Nanoparticles. *Small* **2010**, *6*, 1669–1678.

4. Duncan, R. Polymer Conjugates as Anticancer Nanomedicines. *Nat. Rev. Cancer* **2006**, *6*, 688–701.

5. Chen, J.; Spear, S.; Huddleston, J.; Rogers, R. Polyethylene Glycol and Solutions of Polyethylene Glycol as Green Reaction Media. *Green Chem.* **2005**, *7*, 64–82.

6. Haag, R.; Kratz, F. Polymer Therapeutics: Concepts and Applications. *Angew. Chem. Int. Ed.* **2006**, *45*, 1198–1215.

7. Knop, K.; Hoogenboom, R.; Fischer, D.; Schubert, U. S. Poly(ethylene glycol) in Drug Delivery: Pros and Cons as Well as Potential Alternatives. *Angew. Chem. Int. Ed.* **2010**, *49*, 6288–6308.

8. Harris, J.; Chess, R. Effect of Pegylation on Pharmaceuticals. *Nat. Rev. Drug Discov.* **2003**, *2*, 214–221.

9. Mei, B. C.; Susumu, K.; Medintz, I. L.; Mattoussi, H. Polyethylene Glycol-Based Bidentate Ligands to Enhance Quantum Dot and Gold Nanoparticle Stability in Biological Media. *Nat. Protoc.* **2009**, *4*, 412–423.

10. Vlashi, E.; Kelderhouse, L. E.; Sturgis, J. E.; Low, P. S. Effect of Folate-Targeted Nanoparticle Size on Their Rates of Penetration into Solid Tumors. *ACS Nano* **2013**, *7*, 8573–8582.

11. Burdick, J. A.; Murphy, W. L. Moving from Static to Dynamic Complexity in Hydrogel Design. *Nat. Commun.* **2012**, *3*, 1269.

12. Burdick, J.; Khademhosseini, A.; Langer, R. Fabrication of Gradient Hydrogels Using a Microfluidics/Photopolymerization Process. *Langmuir* **2004**, *20*, 5153–5156.

13. Kingshott, P.; Griesser, H. Surfaces that Resist Bioadhesion. *Curr. Opin. Solid State Mater. Sci.* **1999**, *4*, 403–412.

14. Prime, K.; Whitesides, G. Self-Assembled Organic Monolayers - Model Systems for Studying Adsorption of Proteins at Surfaces. *Science* **1991**, *252*, 1164–1167.

15. Stuart, M. A. C.; Huck, W. T. S.; Genzer, J.; Mueller, M.; Ober, C.; Stamm, M.; Sukhorukov, G. B.; Szleifer, I.; Tsukruk, V. V.; Urban, M.; Winnik, F.; Zauscher, S.; Luzinov, I.; Minko, S. Emerging Applications of Stimuli-Responsive Polymer Materials. *Nat. Mater.* **2010**, *9*, 101–113.

16. Tanaka, M.; Sackmann, E. Polymer-Supported Membranes as Models of the Cell Surface. *Nature* **2005**, *437*, 656–663.

17. Schneider, C.; Jusufi, A.; Farina, R.; Li, F.; Pincus, P.; Tirrell, M.; Ballauff, M. Microsurface Potential Measurements: Repulsive Forces Between Polyelectrolyte Brushes in the Presence of Multivalent Counterions. *Langmuir* **2008**, *24*, 10612–10615.

18. Ruzette, A.; Leibler, L. Block Copolymers in Tomorrow's Plastics. *Nat. Mater.* **2005**, *4*, 19–31.

19. Flory, P. *Principles of Polymer Chemistry*; Baker lectures 1948; Cornell University Press, 1953.

20. de Gennes P.G., *Scaling Concepts in Polymer Physics*; Cornell University Press, 1979.

21. Smith, S.; Finzi, L.; Bustamante, C. Direct Mechanical Measurements of the Elasticity of Single DNA-Molecules by Using Magnetic Beads. *Science* **1992**, *258*, 1122–1126.

22. Marko, J.; Siggia, E. Stretching DNA. *Macromolecules* **1995**, *28*, 8759–8770.

23. Russell, T. Surface-Responsive Materials. *Science* **2002**, *297*, 964–967.

24. Heymann, B.; Grubmuller, H. Elastic Properties of Poly(ethylene-Glycol) Studied by Molecular Dynamics Stretching Simulations. *Chem. Phys. Lett.* **1999**, *307*, 425–432.

25. Kreuzer, H.; Grunze, M. Stretching of Single Polymer Strands: A First-Principles Theory. *Europhys. Lett.* **2001**, *55*, 640–646.

26. Bekiranov, S.; Bruinsma, R.; Pincus, P. Solution Behavior of Polyethylene Oxide in Water as a Function of Temperature and Pressure. *Phys Rev E* **1997**, *55*, 577–585.

27. Gensler, M.; Eidamshaus, C.; Galstyan, A.; Knapp, E.-W.; Reissig, H.-U.; Rabe, J. P. Mechanical Rupture of Mono- and Bivalent Transition Metal Complexes in Experiment and Theory. *J. Phys. Chem. C* **2015**, *119*, 4333–4343.

28. Hugel, T.; Rief, M.; Seitz, M.; Gaub, H.; Netz, R. Highly Stretched Single Polymers: Atomic-Force-Microscope Experiments versus Ab-Initio Theory. *Phys. Rev. Lett.* **2005**, *94*, 048301.

29. Lee, H.; Venable, R. M.; MacKerell, A. D., Jr.; Pastor, R. W. Molecular Dynamics Studies of Polyethylene Oxide and Polyethylene Glycol: Hydrodynamic Radius and Shape Anisotropy. *Biophys. J* . **2008**, *95*, 1590–1599.

30. Vorobyova, I.; Anisimov, V. M.; Greene, S.; Venable, R. M.; Moser, A.; Pastor, R. W.; MacKerell, A. D. Additive and Classical Drude Polarizable Force Fields for Linear and Cyclic Ethers. *J. Chem. Theory Comput.* **2007**, *3*, 1120–1133.

31. Dittmore, A.; McIntosh, D. B.; Halliday, S.; Saleh, O. A. Single-Molecule Elasticity Measurements of the Onset of Excluded Volume in Poly(Ethylene Glycol). *Phys. Rev. Lett.* **2011**, *107*, 148301.

32. Grosberg, A. Y.; Khokhlov, A. R. *Statistical Physics of Macromolecules*; AIP Press, 1994.

33. Livadaru, L.; Netz, R.; Kreuzer, H. Stretching Response of Discrete Semiflexible Polymers. *Macromolecules* **2003**, *36*, 3732–3744.

34. Hanke, F.; Serr, A.; Kreuzer, H. J.; Netz, R. R. Stretching Single Polypeptides: The Effect of Rotational Constraints in the Backbone. *Eur. Polym. J.* **2010**, *92*, 53001.

35. Tsapikouni, T. S.; Missirlis, Y. F. Measuring the Force of Single Protein Molecule Detachment from Surfaces with AFM. *Colloids Surf., B* **2010**, *75*, 252–259.

36. Gomez-Casado, A.; Dam, H. H.; Yilmaz, M. D.; Florea, D.; Jonkheijm, P.; Huskens, J. Probing Multivalent Interactions in a Synthetic Host-Guest Complex by Dynamic Force Spectroscopy. *J. Am. Chem. Soc.* **2011**, *133*, 10849–10857.

37. Nakahara, Y.; Mitani, H.; Kado, S.; Kimura, K. Single-Molecule Force Spectroscopic Study on Chiral Recognition of Cysteine Derivatives Immobilized on a Gold Substrate by Using AFM

Tips Chemically Modified with Optically Active Crown Ethers. *RSC Adv.* **2014**, *4*, 57850–57854.

38. Devanand, K.; Selser, J. Asymptotic-Behavior and Long-Range Interactions in Aqueous-Solutions of Poly(Ethylene Oxide). *Macromolecules* **1991**, *24*, 5943–5947.

39. Kohn, J.; Millett, I.; Jacob, J.; Zagrovic, B.; Dillon, T.; Cingel, N.; Dothager, R.; Seifert, S.; Thiyagarajan, P.; Sosnick, T.; Hasan, M.; Pande, V.; Ruczinski, I.; Doniach, S.; Plaxco, K. Random-Coil Behavior and the Dimensions of Chemically Unfolded Proteins. *Proc. Natl. Acad. Sci. USA* **2004**, *101*, 12491–12496.

40. Blavatska, V.; von Ferber, C.; Holovatch, Y. Shapes of Macromolecules in Good Solvents: Field Theoretical Renormalization Group Approach. *Condens. Matter Phys.* **2011**, *14*, 33701.

41. Sotomayor, M.; Schulten, K. Single-Molecule Experiments in Vitro and in Silico. *Science* **2007**, *316*, 1144–1148.

42. Erdmann, M.; David, R.; Fornof, A.; Gaub, H. E. Electrically Controlled DNA Adhesion. *Nature Nanotech.* **2010**, *5*, 154–159.

43. Baumann, F.; Bauer, M. S.; Milles, L. F.; Alexandrovich, A.; Gaub, H. E.; Pippig, D. A. Monovalent Strep-Tactin for Strong and Site-Specific Tethering in Nanospectroscopy. *Nature Nanotech.* **2016**, *11*, 89?94.

44. Oesterhelt, F.; Rief, M.; Gaub, H. E. Single Molecule Force Spectroscopy by AFM Indicates Helical Structure of Poly(ethylene-Glycol) in Water. *New J. Phys* **1999**, *1*, 6.1?6.11.

45. Xue, Y.; Li, X.; Li, H.; Zhang, W. Quantifying Thiol-Gold Interactions Towards the Efficient Strength Control. *Nat. Commun.* **2014**, *5*, 4348.

46. Kienberger, F.; Raab, A.; Kada, G.; Gruber, H.; Pastushenko, V.; Badt, D.; Schindler, H.; Hinterdorfer, P. Contact and Macmode Molecular Recognition Force Microscopy (MRFM): Force Spectroscopy of Polyethylene Glycol. *Biophys. J* . **2000**, *78*, 381.

47. Kumar, S.; Bouzida, D.; Swendsen, R.; Kollman, P.; Rosenberg, J. The Weighted Histogram Analysis Method for Free-Energy Calculations on Biomolecules. 1. The Method. *J. Comput. Chem.* **1992**, *13*, 1011–1021.

48. Bandyopadhyay, S.; Tarek, M.; Lynch, M.; Klein, M. Molecular Dynamics Study of the Poly(oxyethylene) Surfactant C12E2 and Water. *Langmuir* **2000**, *16*, 942–946.

49. Wehrl, A. General Properties of Entropy. *Rev. Mod. Phys.* **1978**, *50*, 221–260.

50. Fixman, M.; Kovac, J. Polymer Conformational Statistics. 3. Modified Gaussian Models of Stiff Chains. *J. Chem. Phys.* **1973**, *58*, 1564–1568.

51. Malcom, G.; Rowlinson, J. The Thermodynamic Properties of Aqueous Solutions of Polyethylene Glycol, Polypropylene Glycol and Dioxane. *Trans. Faraday Soc.* **1957**, *53*, 921–931.

52. Derkaoui, N.; Said, S.; Grohens, Y.; Olier, R.; Privat, M. PEG400 Novel Phase Description in Water. *J. Colloid Interface Sci.* **2007**, *305*, 330–338.

53. Granick, S.; Bae, S. C. Chemistry A Curious Antipathy for Water. *Science* **2008**, *322*, 1477–1478.

54. Safran, S. A. *Statistical Thermodynamics of Surfaces, Interfaces, and Membranes*; Frontiers in Physics, 2003.

55. Patel, A. J.; Varilly, P.; Jamadagni, S. N.; Acharya, H.; Garde, S.; Chandler, D. Extended Surfaces Modulate Hydrophobic Interactions of Neighboring Solutes. *Proc. Natl. Acad. Sci. USA* **2011**, *108*, 17678–17683.

56. Li, I. T. S.; Walker, G. C. Interfacial Free Energy Governs Single Polystyrene Chain Collapse in Water and Aqueous Solutions. *J. Am. Chem. Soc.* **2010**, *132*, 6530–6540.

57. Bauer, M.; Kekicheff, P.; Iss, J.; Fajolles, C.; Charitat, T.; Daillant, J.; Marques, C. M. Sliding Tethered Ligands Add Topological Interactions to the Toolbox of Ligand-Receptor Design. *Nat. Commun.* **2015**, *6*.

58. Shan, M.; Bujotzek, A.; Abendroth, F.; Wellner, A.; Gust, R.; Seitz, O.; Weber, M.; Haag, R. Conformational Analysis of Bivalent Estrogen Receptor Ligands: From Intramolecular to Intermolecular Binding. *ChemBioChem* **2011**, *12*, 2587–2598.

59. Marszalek, P. E.; Dufrene, Y. F. Stretching Single Polysaccharides and Proteins Using Atomic Force Microscopy. *Chem. Soc. Rev.* **2012**, *41*, 3523–3534.

60. Nettels, D.; Mueller-Spaeth, S.; Kuester, F.; Hofmann, H.; Haenni, D.; Rueegger, S.; Reymond, L.; Hoffmann, A.; Kubelka, J.; Heinz, B.; Gast, K.; Best, R. B.; Schuler, B. Single-Molecule Spectroscopy of the Temperature-Induced Collapse of Unfolded Proteins. *Proc. Natl. Acad. Sci. USA* **2009**, *106*, 20740–20745.

61. Cui, S.; Pang, X.; Zhang, S.; Yu, Y.; Ma, H.; Zhang, X. Unexpected Temperature-Dependent Single Chain Mechanics of Poly(N-isopropyl-acrylamide) in Water. *Langmuir* **2012**, *28*, 5151–5157.

62. Krysiak, S.; Wei, Q.; Rischka, K.; Hartwig, A.; Haag, R.; Hugel, T. Adsorption Mechanism and Valency of Catechol-Functionalized Hyperbranched Polyglycerols. *Beilstein J. Org. Chem.* **2015**, *11*, 828–836.

63. Krysiak, S.; Liese, S.; Netz, R. R.; Hugel, T. Peptide Desorption Kinetics from Single Molecule Force Spectroscopy Studies. *J. Am. Chem. Soc.* **2014**, *136*, 688–697.

64. Pirzer, T.; Hugel, T. Atomic Force Microscopy Spring Constant Determination in Viscous Liquids. *Rev. Sci. Instrum.* **2009**, *80*, 035110.

65. Hutter, J.; Becherhoeffer, J. Calibration of Atomic-Force-Microscope Tips. *Rev. Sci. Instrum.* **1993**, *64*, 3342.

66. Frisch, M. J.; Trucks, G. W.; Schlegel, H. B.; Scuseria, G. E.; Robb, M. A.; Cheeseman, J. R.; Scalmani, G.; Barone, V.; Mennucci, B.; Petersson, G. A.; Nakatsuji, H.; Caricato, M.; Li, X.; Hratchian, H. P.; Izmaylov, A. F.; Bloino, J.; Zheng, G.; Sonnenberg, J. L.; Hada, M.; Ehara, M. et al. Gaussian-09 Revision D.01. Gaussian Inc. Wallingford CT 2009.

67. Zhao, Y.; Truhlar, D. G. The M06 Suite of Density Functionals for Main Group Thermochemistry, Thermochemical Kinetics, Noncovalent Interactions, Excited States, and Transition Elements: Two New Functionals and Systematic Testing of Four M06-Class Functionals and 12 Other Functionals. *Theor. Chem. Acc.* **2008**, *120*, 215–241, Meeting on Practicing Chemistry with Theoretical Tools, Maui, HI, JAN 15-18, 2007.

68. Dunning, T. Gaussian-Basis Sets for Use in Correlated Molecular Calculations. 1. The Atoms Boron Through Neon and Hydrogen. *J. Chem. Phys.* **1989**, *90*, 1007–1023.

69. Van der Spoel, D.; Lindahl, E.; Hess, B.; Groenhof, G.; Mark, A.; Berendsen, H. GROMACS: Fast, Flexible, and Free. *J. Comput. Chem.* **2005**, *26*, 1701–1718.

70. Bussi, G.; Donadio, D.; Parrinello, M. Canonical Sampling Through Velocity Rescaling. *J. Chem. Phys.* **2007**, *126*, 014101.

71. Parrinello, M.; Rahman, A. Polymorphic Transitions in Single-Crystals - a New Malecular-Dynamics Method. *J. Appl. Phys.* **1981**, *52*, 7182–7190.

72. Luzar, A.; Chandler, D. Structure and Hydrogen-Bond Dynamics of Water-Dimethyl Sulfoxide Sulfoxide Mixtures by Computer-Simulations. *J. Chem. Phys.* **1993**, *98*, 8160–8173.

Graphical TOC Entry